Journal of the Mechanical Behavior of Biomedical Materials 81 (2018) 26–38

Contents lists available at ScienceDirect

Journal of the Mechanical Behavior of Biomedical Materials

journal homepage: www.elsevier.com/locate/jmbbm

Titanium surface bio-functionalization using osteogenic peptides: Surface chemistry, biocompatibility, corrosion and tribocorrosion aspects

Luciana D. Trino[a], Erika S. Bronze-Uhle[a], Amsaveni Ramachandran[b], Paulo N. Lisboa-Filho[a,*], Mathew T. Mathew[c], Anne George[b]

[a] São Paulo State University (Unesp), School of Sciences, Bauru, SP 17033-360, Brazil
[b] Department of Oral Biology, College of Dentistry, University of Illinois at Chicago, Chicago, IL, 60612, USA
[c] Department of Biomedical Sciences, College of Medicine at Rockford, University of Illinois-School of Medicine at Rockford, Rockford, IL, 61107-1897, USA

ARTICLE INFO

Keywords:
Titanium dioxide
Osteogenic peptides
Human mesenchymal stem cells
Tribocorrosion
Functional materials

ABSTRACT

Titanium (Ti) is widely used in biomedical devices due to its recognized biocompatibility. However, implant failures and subsequent clinical side effects are still recurrent. In this context, improvements can be achieved by designing biomaterials where the bulk and the surface of Ti are independently tailored. The conjugation of biomolecules onto the Ti surface can improve its bioactivity, thus accelerating the osteointegration process.

Ti was modified with TiO_2, two different spacers, 3-(4-aminophenyl) propionic acid (APPA) or 3-mercapto-propionic acid (MPA) and dentin matrix protein 1 (DMP1) peptides. X-ray photoelectron spectroscopy analysis revealed the presence of carbon and nitrogen for all samples, indicating a success in the functionalization process. Furthermore, DMP1 peptides showed an improved coverage area for the samples with APPA and MPA spacers. Biological tests indicated that the peptides could modulate cell affinity, proliferation, and differentiation. Enhanced results were observed in the presence of MPA. Moreover, the immobilization of DMP1 peptides through the spacers led to the formation of calcium phosphate minerals with a Ca/P ratio near to that of hydroxyapatite. Corrosion and tribocorrosion results indicated an increased resistance to corrosion and lower mass loss in the functionalized materials, showing that this new type of functional material has attractive properties for biomaterials application.

1. Introduction

Titanium and its alloys are widely used in dental and orthopedic implants due to their adequate biocompatibility, high corrosion resistance, and high strength-to-weight ratio. This combination of properties is required for load-bearing applications (Alves et al., 2015). Unfortunately, despite the positive bulk performance, there is still an undesirable number of implant failures. Dental implants failures are around 1–20% (Alves et al., 2017), whereas for orthopedic implants this number is higher than 35% (Tobin, 2017).

To overcome such concerns, implant longevity could be achieved by designing biomaterials where the bulk and the surface are independently tailored with regenerative capabilities. The biocompatibility, as well as the biocorrosion resistance of titanium, is closely related to the properties (e.g., structure, morphology and composition) of a surface oxide layer (Li et al., 2004). Once the surface of the synthetic device is in direct contact with a living organism, biocompatibility becomes a critical requirement in any biomaterial (Silva-Bermudez and Rodil, 2013; Silva-Bermudez et al., 2013).

Strict attention must be paid to the surface of a material system, as its reaction with the host tissue is often the key factor in the success or failure of implantation (Bauer et al., 2013). Various physical and chemical modifications of the Ti surface have been proposed in order to obtain the most biocompatible implant surface (Li et al., 2004; Rafieerad et al., 2015; Wang et al., 2016a, 2016b; Sun et al., 2016; Jemat et al., 2015). Nanostructured metal oxide coatings, such as TiO_2, have shown good results in the protein interaction procedure. Consequently, this is the first step in the initial process of the material's interaction with the biological environment (Kumari et al., 2010).

Reactive functional groups can easily adhere to the titanium (coated with metal oxides), thus yielding surfaces with greater stability and functionality. The introduction of polymer-grafted surfaces or self-assembled monolayers (SAM) produced advances in this field (Tanaka et al., 2007, 2008; Suh et al., 2004; Hanawa, 2010; Zhang et al., 2010; Ma et al., 2013; Balasundaram et al., 2008; Cai et al., 2006). The metal oxide-functionalized surfaces affect the adsorption of biomolecules, like

* Corresponding author.
E-mail address: plisboa@fc.unesp.br (P.N. Lisboa-Filho).

https://doi.org/10.1016/j.jmbbm.2018.02.024
Received 26 December 2017; Received in revised form 17 February 2018; Accepted 17 February 2018
Available online 21 February 2018
1751-6161/

proteins and peptides. These surfaces also impact some important cell behavior, like cell spreading and migration (Silva-Bermudez and Rodil, 2013; Advincula et al., 2005).

Proteins from the extracellular matrix (ECM) provide instructional cues for cellular differentiation, migration, wound healing, and immune response (Ravindran and George, 2014). Specifically, functional extracellular matrix proteins contribute to the formation and maintenance of mineralized tissues – like dentin and bone. Dentin matrix protein 1 (DMP1) is an acidic, non-collagenous phosphoprotein, that plays a crucial role in osteoblast/odontoblast differentiation and mineral nucleation events (Ravindran and George, 2014; He et al., 2005; Bhatia et al., 2012). Certain specific extracellular matrix proteins, such as DMP1, act as nucleators for hydroxyapatite formation.

Acidic clusters in matrix proteins play a precise molecular role in mineral surface recognition. He et al. (2003), investigated the acidic domains of DMP1, and determined that the peptides ESQES and QESQSEQDS induce the formation of plate-shaped apatite crystals. Notably, ESQES and QESQSEQDS are both derivatives of DMP1. Once DMP1 peptides stimulate the acceleration and enhancement of osteointegration, osteoblast differentiation, and matrix production, an osteo-inductive effect may be promoted on the implanted material (Frosch et al., 2003).

The following describes improvements in the DMP1 peptides' adhesion process onto functionalized metal oxide surfaces. This process might improve the osteointegration of an implanted material. The spacers employed consist of two bifunctional molecules: 3-(4-aminophenyl) propionic acid (APPA) and 3-mercaptopropionic acid (MPA) (Trino et al., 2018). The interactions between the oxide/organic molecules and organic molecules/peptides were evaluated, and the samples were characterized by X-ray Photoelectron Spectroscopy (XPS) and Atomic Force Microscopy (AFM). These metal oxide surfaces have functional groups that may interact with amino or carboxyl groups from DMP1 peptides.

To analyze the material cytotoxicity, cell proliferation, and differentiation, in-vitro tests with human mesenchymal stem cells were developed. Corrosion and tribocorrosion tests validated the importance of mechanical properties in implants, because once metal starts to degrade, inflammation and implant failure can follow. The use of a functionalized material with DMP1 peptides, which may act as a translator between the surface properties of the material and the cell receptors, is a strong factor in the performance and overall survivability of the implant in the biological environment.

2. Materials and methods

2.1. Titanium dioxide deposition

The titanium dioxide was synthesized by sol-gel method (Oskam et al., 2003). The oxide deposition was performed by spin coating technique (2000 RPM per 60 s) under ambient conditions. Titanium dioxide was annealed at 850 °C for two hours in a heating rate of 1 °C min^{-1} in order to obtain a rutile crystalline polymorphic phase. The obtained TiO_2 film was uniform with thickness around 500 nm (Fig. S1). TiO_2 surface was functionalized with two different bifunctional molecules 3-mercaptopropionic acid (MPA) and 3–4 aminophenyl propionic acid (APPA) by immersion method as described in previous work (Trino et al., 2018).

2.2. Peptides deposition

Peptides pA (ESQES) and pB (QESQSEQDS) derived from dentin matrix protein 1 (DMP1) were synthesized via solid phase. The peptides were diluted in the ratio 1 of pA to 4 of pB in PBS and carbonate buffer solution, in order to have a concentration of 1 mg/mL. The samples were placed in a 24 well plate and covered with the peptides solution. In order to form the crosslink between the peptides, the samples were maintained overnight under UV-light in steric conditions.

2.3. Cell culture

Human mesenchymal stem cells containing the gene for Green Fluorescence Protein (hMSCs-GFP) were seeded (2×10^4 cells) upon the samples in an incubator under 37 °C and CO_2 concentration of 5% for 24 h and seven days, until they were confluent. The complete media was prepared with α-MEM, 20% of FBS, L-glutamin and antibiotic.

2.4. Cell attachment test

To analyze the attachment of the cells upon the substrate after 24 h and 7 days of culture, hMSC-GFP cells were fixed with buffered neutral formalin 10% and imaged by confocal fluorescence microscopy (Zeiss LSM 710) applying a magnification of 20 × .

2.5. Cell proliferation assay

A colorimetric method for determining the number of viable cells in proliferation or cytotoxicity assays was performed using a CellTiter 96® AQueous One Solution Cell Proliferation Assay (PROMEGA) kit. The cells were cultured for 1, 3 and 5 days in triplicates. The plates were read in a Synergy 2 multi-mode plate reader at 490 nm. The quantity of formazan product measured by absorbance at 490 nm was directly proportional to the number of living cells in culture.

2.6. In vitro nucleation test

Nucleation was carried out under high concentrations of calcium and phosphate. The samples were immersed in a 1 M calcium chloride solution for a period of 30 min. They were then washed extensively in water to remove any nonspecifically bound calcium and then immersed in a 1 M sodium phosphate solution for a period of 30 min. Finally, they were washed with water and dehydrated with 20%, 30%, 40%, 50%, 70%, 80%, 90% and 100% of ethanol solution and then dried with hexamethyldisilazane (HMDS).

2.7. Quantitative real-time polymerase chain reaction (QRT-PCR) studies

Purification of total RNA from hMSC-GFP cells using spin technology was performed for 2.5×10^4 cells seeded upon the substrates per 7 days. Two sets of samples was analyzed, one with an osteogenic media and a control with standard media. The cells were disrupted in a lysis buffer and homogenized. Ethanol was then added to the lysate, creating conditions that promote selective binding of RNA to the RNeasy kit membrane (Qiagen). The sample was then applied to the RNeasy Mini spin column. Total RNA binds to the membrane, contaminants were efficiently washed away, and high-quality RNA was eluted in RNase-free water. All bind, wash, and elution steps were performed by centrifugation in a microcentrifuge. The solutions were placed in a 96 well plate to be read in triplicates in a real-time PCR Reader (StepOnePlus, Applied Biosystems).

2.8. Corrosion tests

The electrochemical test was conducted using a standard three-electrode corrosion cell, PBS as electrolyte and a potentiostat (G700, Gamry Inc.) to perform the corrosion experiments on the samples in triplicates. More details can be found at the Supporting information.

2.9. Tribocorrosion tests

The samples were subjected to tribocorrosion testing using a tribometer (Advanced Linear Reciprocating Tribometer, Ducom Instruments). A standard three-electrode corrosion cell and a

Table 1
Measured binding energies (BE), full widths at half maximum (FWHM), the proportion of atomic composition and chi-square goodness-of-fit (χ^2) by XPS analysis.

Sample	Signal	Peak	Assignment	BE (eV)	FWHM	Atomic Composition (%)	χ^2
Ti P	C 1s					26.2	1.1
		C_1	C-H	283.7	2	5.1	
		C_2	C-C	285.0	1.4	74.8	
		C_3	C-N	286.6	1.6	11.0	
		C_5	COOH	288.7	1.9	9.1	
	O 1s					42.3	1.5
		O_1	Ti-O	530.1	1.1	38.9	
				530.9	2.2	53.7	
		O_3	H_2O/C-OH	533.1	2.0	2.8	
		O_4	Na Auger peak	536.1	1.3	4.5	
	N 1s					0.33	0.77
		N_1	Ti-N	398.1	1.7	8.6	
		N_3	C-NH_2	400.3	1.4	91.4	
TiO_2 P	C 1s					28.3	1.3
		C_1	C-H	283.7	1.7	2.3	
		C_3	C-N	285.5	1.3	69.4	
		C_4	C-OH	287.1	1.4	17.9	
		C_5	COOH	288.8	1.5	10.4	
	O 1s					42.0	
		O_1	Ti-O	528.5	1.1	1.3	1.3
				529.9	1.1	50.9	
		O_2	O-H/C-O	531.1	1.6	29.9	
		O_3	H_2O/ C-OH	532.7	2.1	12.5	
		O_4	Na Auger peak	536.3	2.3	5.4	
	N 1s					1.2	1.0
		N_2	C-N	398.9	1.5	6.0	
		N_3	C-NH_2	400.6	2.5	94	
TiO_2 MPA P	C 1s					25.2	2.0
		C_1	C-H	283.8	1.7	3.3	
		C_3	C-N	285.6	1.4	68.5	
		C_4	C-OH	287.0	1.3	11.4	
		C_5	COOH	288.9	2.1	16.8	
	O 1s					34.6	2.0
		O_1	Ti-O	529.9	1.1	34.5	
		O_2	O-H/C-O	531.3	1.5	33.7	
		O_3	H_2O/C-OH/S-O	532.8	2.1	18.8	
		O_4	Na Auger peak	536.6	2.1	13.0	
	N 1s					1.7	0.8
		N_2	C-N	398.9	1.7	16.79	
		N_3	C-NH_2	400.7	1.5	74.2	
		N_4	-NH_3^+	403.3	1.9	3.9	
TiO_2 APPA P	C 1s					33.8	2.1
		C_1	C-H	283.7	2.5	5.0	
		C_3	C-N	285.6	1.3	67.3	
		C_4	C-OH	287.0	1.3	12.8	
		C_5	COOH	288.8	1.9	14.9	
	O 1s					32.0	2.2
		O_1	Ti-O	529.9	1.0	28.9	
		O_2	O-H/C-O	531.3	2.3	51.4	
		O_3	H_2O/ C-OH	533.4	1.6	6.8	
		O_4	Na Auger peak	536.6	2.1	12.9	
	N 1s					1.6	1.1
		N_2	C-N	398.9	2.0	12.9	
		N_3	C-NH_2	400.6	1.6	87.1	

potentiostat (G700, Gamry Inc.) were linked to the tribocorrosion system. The working electrode consisted of the sample with an exposed area of 1.0 cm^2, an SCE was used as the reference electrode, and the counter electrode was a graphite rod. The electrolyte used was 15 mL of PBS. The samples were analyzed in triplicates. More details can be found at the Supporting information.

3. Results and discussion

3.1. Bio-functionalization analysis

Covalent binding of DMP1 peptides and the titanium dioxide surface was achieved via the use of two different spacers, APPA ($H_2NC_6H_4CH_2CH_2CO_2H$) and MPA ($HSCH_2CH_2CO_2H$). Both spacers had a surface-attaching head group and a peptide-binding tail group. The surface chemical compositions of the controls and functionalized Ti surfaces were confirmed through XPS investigations. The Ti $2p_{3/2}$ peak, present at a binding energy of 458.8 eV corresponding to the Ti(IV) of TiO_2 (Moulder, 1992), was used for the energy calibration of all the spectra. XPS results are shown in Table 1 and more detailed data can be found in Fig. S2-S5.

Pristine Ti and TiO_2 surfaces indicated the presence of new elements, (C) and (N), which were introduced by the DMP1 peptides. For the samples functionalized with MPA, the presence of N 1s confirmed the adhesion of the peptides. APPA has the elements C and N on its structure. However, no significant changes were evidenced when comparing the C 1s and N 1s spectrum with the other samples. This suggests that chemisorption occurs without substantial modifications on the DMP1 peptides structure for all the samples analyzed.

The core-level spectra of pA (ESQES) and pB (QESQSEQDS) peptides

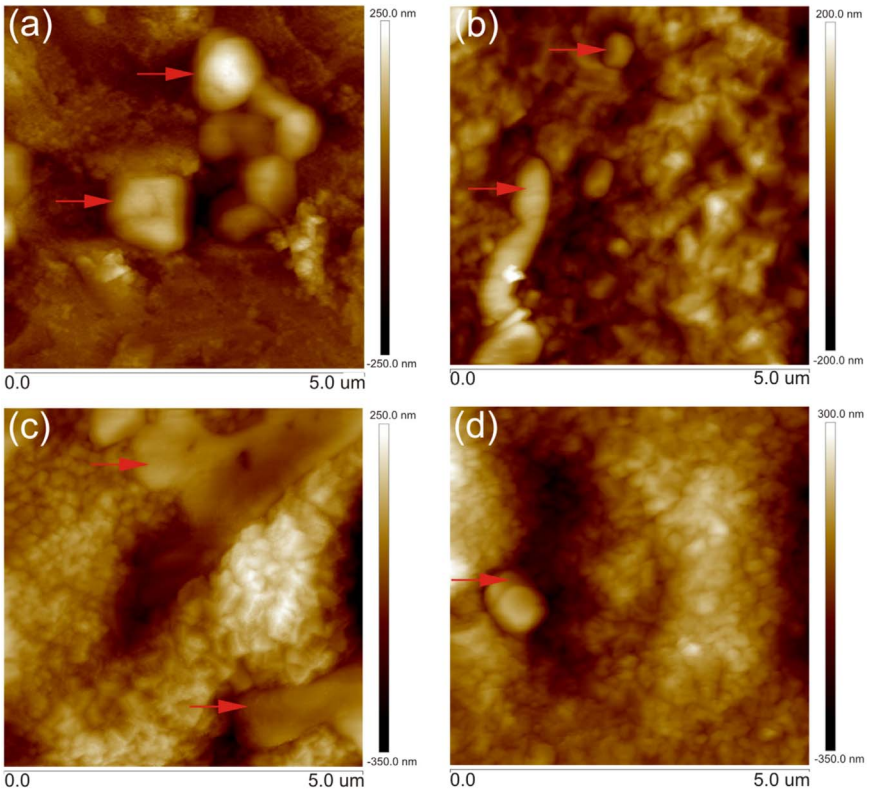

Fig. 1. AFM topography for the samples functionalized with DMP1 peptides: Ti P (a), TiO_2 P (b), TiO_2 APPA P (c) and TiO_2 MPA P (d). The red arrows show some of the aggregated peptides structures present in the samples Ti P, TiO_2 P and TiO_2 MPA P, and a DMP1 peptide multilayer deposition in the TiO_2 APPA P sample.

derived from DMP1 are identical, and they have a nearly indistinguishable amino acid composition. Various components, labeled in order of rising binding energy, comprise these amino acids. The C 1s peak results are from five contributions labeled C_1–C_5, varying only for pristine Ti. C_1, C_2, C_3 and C_5 peaks assigned, as C-H (McKenna et al., 2011; Askari et al., 2016), C-C, C-N, and COOH interactions (Moulder, 1992), were indicated through the bare Ti. The samples, functionalized with the oxide and the spacers molecules, present the contributions of C_1, C_3, C_4 and C_5 from the peak of C 1s, where C_4 refers to the C–OH bond. The presence of O 1s results from three contributions (O_1-O_3). They correspond to the oxygens of Ti-O from the TiO_2 surface (O_1), O-H/C-O from the biomolecules (O_2), and O_3, which is H_2O physiosorbed. C-OH results from the biomolecules and S-O, in the case of MPA, contains sulfur.

The samples showed the presence of ions from the phosphate buffer solution (PBS). Sodium Auger peak (Na KLL) presents an interference in the O 1s signal around 536 eV, and has been assigned as O_4. The N 1s spectrum consists of four contributions (N_1-N_4). N_1 represents the Ti-N bond present only in pristine titanium, due to the absence of functional groups to bond with the peptides. N_2 and N_3 correspond to the C-N and C-NH_2 interactions in the DMP1 peptides and the APPA spacer, respectively. N_4 can be assigned to positively charged nitrogens in a large number of environments (-NH_3^+) (Molina et al., 2011).

The atomic percentage of nitrogen is lower for Ti P (0.33%) and TiO_2 P (1.2%), but shows increased values for the samples with MPA (1.7%) and APPA (1.6%). This indicates an efficient peptide immobilization on the Ti surface for all the investigated samples. However, the higher content of N 1 s in the presence of MPA and APPA indicates a preferential attachment of the peptides due to the attraction between the terminal functional groups of the spacers, and the amino or acidic groups on the peptides. As shown in previous work, the APPA molecule bind to the oxide surface by carboxylic acid (-COOH) groups, leading free amine (-NH_2) functionality to bind with -COOH terminal groups from DMP1 peptides (Trino et al., 2018). On the other hand, the MPA molecule adhered to the oxide surface by mercapto (-SH) groups, binding with DMP1 peptides through the -COOH functionality with the -NH_2 terminal group from DMP1 peptides.

Surface topography was examined by AFM for the peptides' immobilization on the control and functionalized samples (Fig. 1). The results indicated that the peptides yielded poor adhesion because they formed agglomerated structures in some regions of the control samples. A uniform layer was formed in the presence of the spacers, but surface clustering was observed for the APPA. The formation of peptide aggregates strongly depends on the experimental conditions, including pH, concentration, and temperature (Gsponer and Vendruscolo, 2006; Enciso et al., 2015).

Due to cooperative effects, attractive forces that lead to positive, cooperative adsorption (Rabe et al., 2011) or surface-dependent conformational changes, can yield macroscopically observable results. The cooperative effects also can enhance the peptides' adsorption, which are mediated by previously adsorbed peptides. The previously adsorbed peptides were tightly connected and displayed surface clustering and aggregation.

The aggregation phenomenon can be explained by the formation of oligomers from pA and pB peptides (He et al., 2003). The isoelectric point (pI) for pA and pB are 3.52 and 3.41, respectively. Those values are lower than the carbonate buffer solution pH (9.2), on which the peptides were kept for functionalization. When the solution pH is higher than the peptides pI, the peptides are negatively charged and they cling closely to each other, thus forming the oligomers. The overall charge density, calculated by GenScript Peptide Property Calculator, for pA is − 3 and for pB is − 4 in carbonate buffer solution pH (Peptide Property Calculator, 2017). In the case of the control samples, the surface was not charged, leading to a preferential agglomeration of the peptides' oligomers and poor surface coverage and adhesion.

The samples functionalized with the MPA and APPA spacers yielded a higher coverage area with good adhesion, due to the attraction between the functional groups of the spacers and the peptides. Moreover,

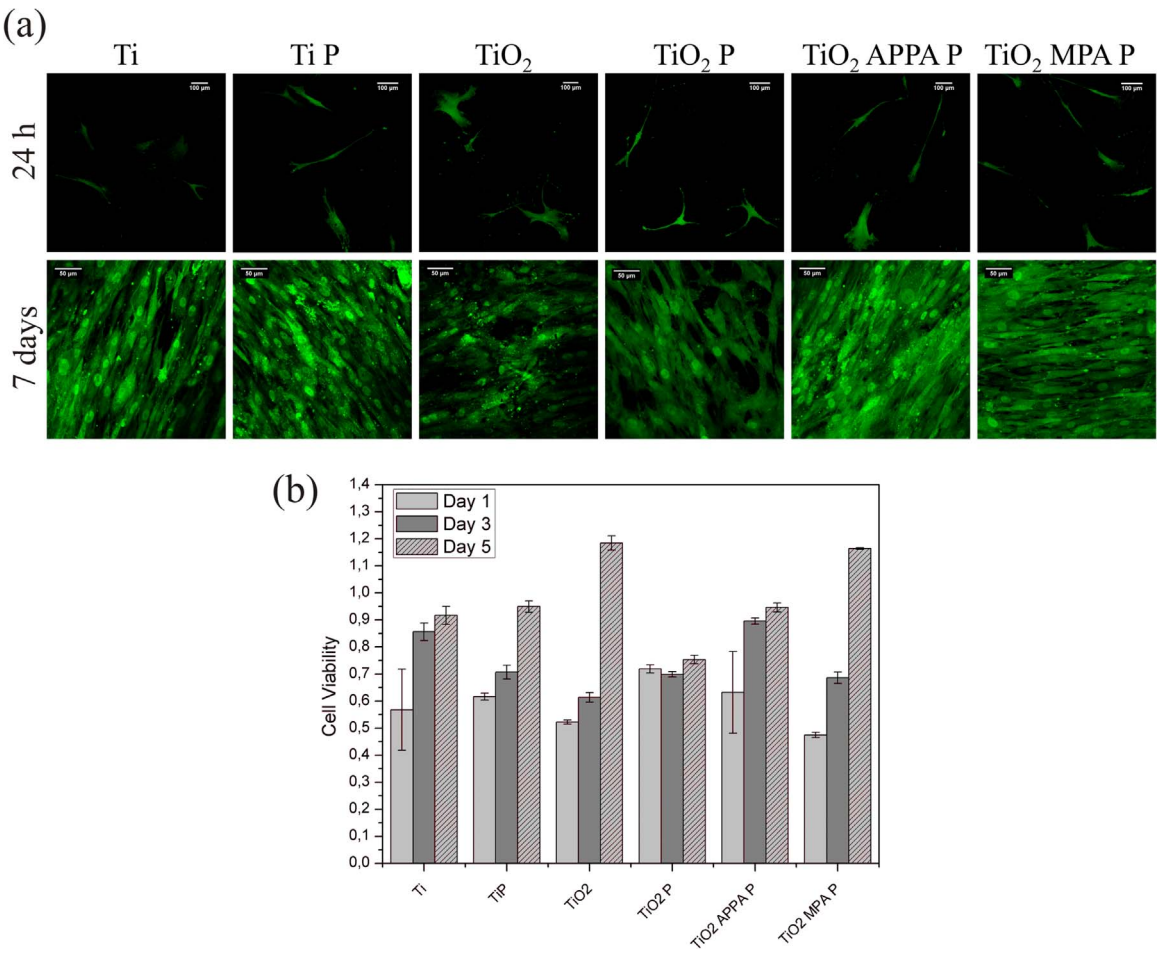

Fig. 2. Fluorescence micrographs of hMSC-GFP cultured upon the control and the functionalized samples in the absence and in the presence of the peptides after 24 h and 7 days (a). Cell viability and proliferation of human mesenchymal stem cells cultured per 1, 3 and 5 days upon the Ti and TiO_2 control samples in the absence and in the presence of DMP1 peptides, and also in the samples containing MPA and APPA spacers with DMP1 peptides (b).

the TiO_2 APPA P sample presented some regions with multilayer deposition. This might be due to the attractive force between the negatively charged peptide and the positive free amine group from the spacer, leading to a multilayer deposition in some regions.

The surface roughness measured by AFM showed that there are no significant changes in arithmetic mean roughness (Ra) for the analyzed samples. The Ra value was 175 (± 13) nm, 192 (± 14) nm, 167 (± 9) nm, and 174 (± 11) nm for the Ti P, TiO_2 P, TiO_2 APPA P and TiO_2 MPA P samples, respectively. Likely the Ra values found, the Ra surface roughness from commercially available dental implants are between 100 and 1000 nm (Sezin et al., 2016; Ramel et al., 2016; Alla et al., 2011).

The surface wettability was analyzed by contact angle, however the surfaces functionalized with the DMP1 peptides were extremely hydrophilic and it was not possible to measure the water contact angle, as shown in Fig. S6 at the Supporting information. The increase in hydrophilicity by the DMP1 peptides functionalization plays an important role in cell behavior. Cells easily adhere and proliferate on superhydrophilic surfaces immediately after seeding (Ishizaki et al., 2010).

3.2. Biological tests

3.2.1. Cell adhesion, spreading and proliferation assay

Cell adhesion and spreading were also examined since they are a critical prerequisite for subsequent functions, such as proliferation and differentiation. The human mesenchymal stem cells, modified with green fluorescence protein (hMSC-GFP), were characterized by confocal fluorescence microscopy after 24 h and after seven days of cell culturing (Fig. 2**a**). Generally, the density of the adherent cells was in the maximum range after the seven day incubation period. No significant difference was observed regarding cell morphology. Moreover, the cells adhered, spread, and exhibited a polarized morphology for the analyzed samples. In addition, the results showed a layer of adherent and viable cells (green fluorescence) with higher growth in the Ti P, TiO_2 APPA P, and TiO_2 MPA P samples functionalized with DMP1 peptides. This indicates that the peptides can modulate cell affinity and can possibly differentiate.

A proliferation assay of hMSC-GFP culture was performed at one, three and five-day intervals to investigate cell viability in the both presence and absence of DMP1 peptides (Fig. 2**b**). These experiments indicated that all samples, with one exception, presented cell growth during the intervals, and no significant cytotoxicity was observed. The observed exception was for TiO_2 P, on which the addition of DMP1 peptides enhanced cell growth on day first. No significant growth was observed after 5 days.

The TiO_2 and MPA P samples showed a higher increase in cell growth when compared with the other groups. TiO_2 is known to increase the biocompatibility of pristine titanium (López-Huerta et al., 2014; Sangeetha et al., 2013), which may be the reason for the hMSC-GFP behavior. In addition, sulfur-containing functional groups, such as the mercapto group in MPA, can affect the behavior of cells. Additionally, the mercapto group in MPA is efficient in stimulating cell adhesion, activating the cell spreading process, and influencing cytoskeleton reorganization (Kowalczyńska and Nowak-Wyrzykowska,

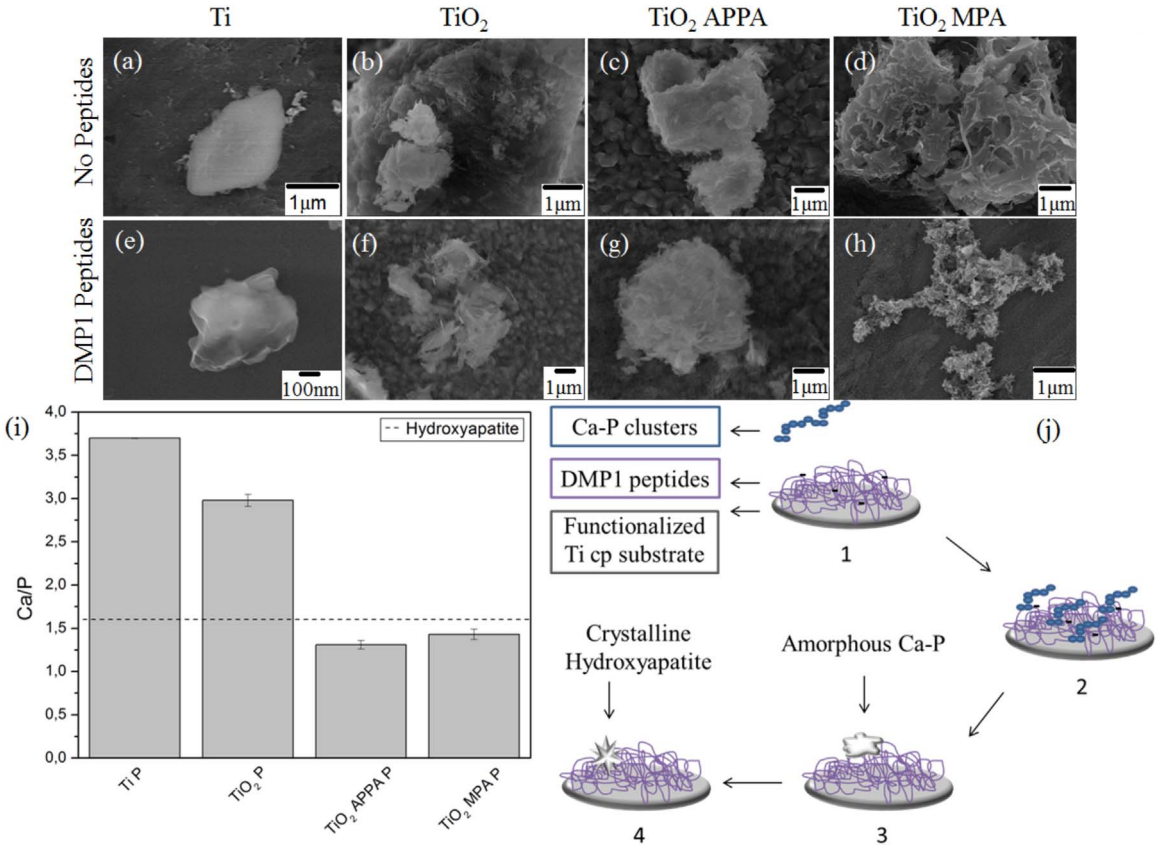

Fig. 3. SEM of calcium phosphate deposits upon the analyzed samples (a-h). Ca/P ratio for the samples functionalized with DMP1 peptides (i). A scheme of HAP nucleation is presented in (j), on which step 1 shows the Ca-P clusters in solution. The clusters aggregation near the surface functionalized with DMP1 peptides is shown in step 2. Step 3 shows the nucleation of amorphous calcium phosphate particles. The crystallization in hydroxyapatite directed by the surface is shown in step 4.

2003). Overall, the samples functionalized with the peptides were capable of modulating cell affinity and proliferation.

3.2.2. *In vitro nucleation assay*

Hydroxyapatite (HAP) is the most important inorganic constituent of human hard tissues (Dumont et al., 2016). Generally, HAP formation is the indicator of bone bioactivity in material, and it further enhances osteointegration of the implant. DMP1 peptides have favorable acidic sites that can induce HAP nucleation, such as glutamic acid, aspartic acid, and serine (Gajjeraman et al., 2007; Padovano et al., 2015; Gorski, 1992).

For the pristine Ti, a solid mineral with a non-specific shape was observed. When comparing the titanium sample with titanium functionalized with peptides, a change in the shape of both minerals was noted. The mineral presents a lamellar shape for Ti P sample. For TiO_2, with and without the peptides, no significant change was observed. However, the functionalized samples presented mineral size with a needle-like morphology. This indicates that DMP1 peptides can stabilize calcium phosphate ions, thus inducing the formation of smaller minerals with a defined morphology. Further, the calculated Ca/P ratio for the samples functionalized with peptides, in the presence of the spacers, was consistent with the ideal atomic ratio of 1.6 in pure HAP (Padovano et al., 2015). See Fig. 3**i**.

The acidic groups present on DMP1 peptides lead to elevated overall negative charge densities on the surface, thus acting as nucleation sites for hydroxyapatite deposition (Gorski, 1992; Alvares, 2014). A diagram of Hydroxyapatite nucleation in the presence of DMP1 peptides is presented in Fig. 3**j**.

In Step One, pre-nucleation clusters of calcium and phosphorus are formed in the solution. As the surface presents a negative charge density, it attracts Ca^{+2} ions from clusters in the solution, thus starting the nucleation (Step Two). The deposition of pre-nucleated clusters leads to a transformation into an amorphous calcium phosphate (Step Three). In Step Four, the amorphous calcium phosphate grows spontaneously by consuming the calcium, phosphate, and hydroxide ions of the surrounding solution, thus crystallizing into bone-like hydroxyapatite with a preferential needle-like morphology (Gajjeraman et al., 2007; Cölfen, 2010).

3.2.3. *Quantitative real-time polymerase chain reaction (QRT-PCR)*

To evaluate the ability of DMP1 peptides in accelerating hMSC osteo-inductive properties, the expression of osteogenic genes was quantified by QRT-PCR on day seven. The marker genes analyzed include alkaline phosphatase (ALP), alpha-1 type-1 collagen (Col1a1), osteopontin (OPN), osteocalcin (OCN), runt-related transcription factor 2 (Runx2), and bone sialoprotein (BSP). All genes were upregulated for the samples containing DMP1 peptides (Fig. 4), indicating that the surface functionalization had a positive influence on hMSCs osteogenic differentiation.

Based on QRT-PCR results, ALP was upregulated by more than 10.2 folds for the samples functionalized with DMP1 peptides. ALP is a calcium and phosphate-binding protein and an osteogenesis enzyme that often presents at high expression levels in osteoblasts (Ruan et al., 2016). Col1a1 showed an increased value for the Ti P sample; however, in the TiO_2 P, TiO_2 APPA P, and TiO_2 MPA P the Col1a1 gene was also upregulated. Col1a1 is the most abundant protein of the extracellular bone matrix and can be considered an early marker for osteogenic differentiation (Shi et al., 2017).

OPN is an important marker of bone remodeling, but it is not identified as a bone-specific protein since it is expressed in other types of tissues. By contrast, OCN is the most specific gene for mineralization in the later stages of osteogenic differentiation (Zheng et al., 2014).

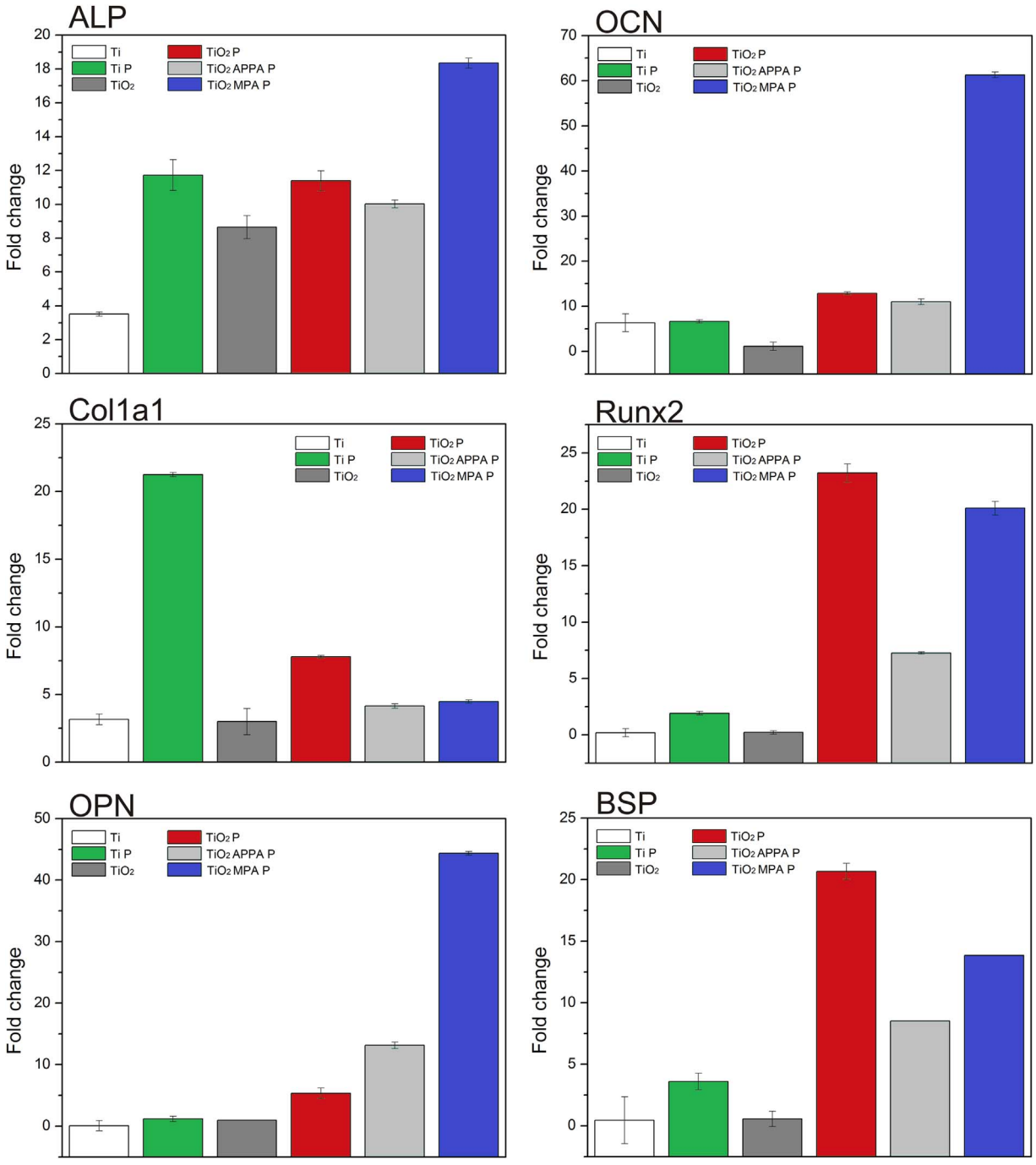

Fig. 4. Expression of osteogenic marker genes for the different samples analyzed by QRT-PCR.

OPN and OCN showed a dramatic increase in the TiO_2 MPA P sample, indicating the rapid induction of cellular differentiation. Runx2 showed a significant upregulation when hMSCs were cultured on the TiO_2 P and TiO_2 MPA P samples. Runx2 is the main osteogenic master-switch gene for osteoblast differentiation (Bedi et al., 2009). BSP is a structural protein that is specifically expressed by fully-differentiated osteoblasts. TiO_2 P and TiO_2 MPA P showed increased BSP expression values, indicating that DMP1 peptides play a crucial role in hMSCs osteogenic differentiation. Therefore, QRT-PCR results confirmed that osteogenic differentiation was dramatically enhanced by DMP1 peptides.

3.3. Electrochemical and mechanical properties

3.3.1. Corrosion

To extend the implant longevity and performance, it is important to investigate the effectiveness of film attachment and organic and biomolecules functionalization. This provides a clearer understanding of the role of corrosion and wear on the tailored materials in medical device applications. The electrochemical properties of the materials were analyzed by electrochemical tests. These tests were performed in the control samples, Ti and TiO_2, and in the Ti P, TiO_2 P, TiO_2 APPA P, and TiO_2 MPA P samples to analyze the behavior of the peptides.

The open circuit potential (OCP), versus time of exposure, is provided in Fig. 5**a**. After a minor initial increase, OCP becomes stable over around 1000 s of exposure. This indicates that no significant change

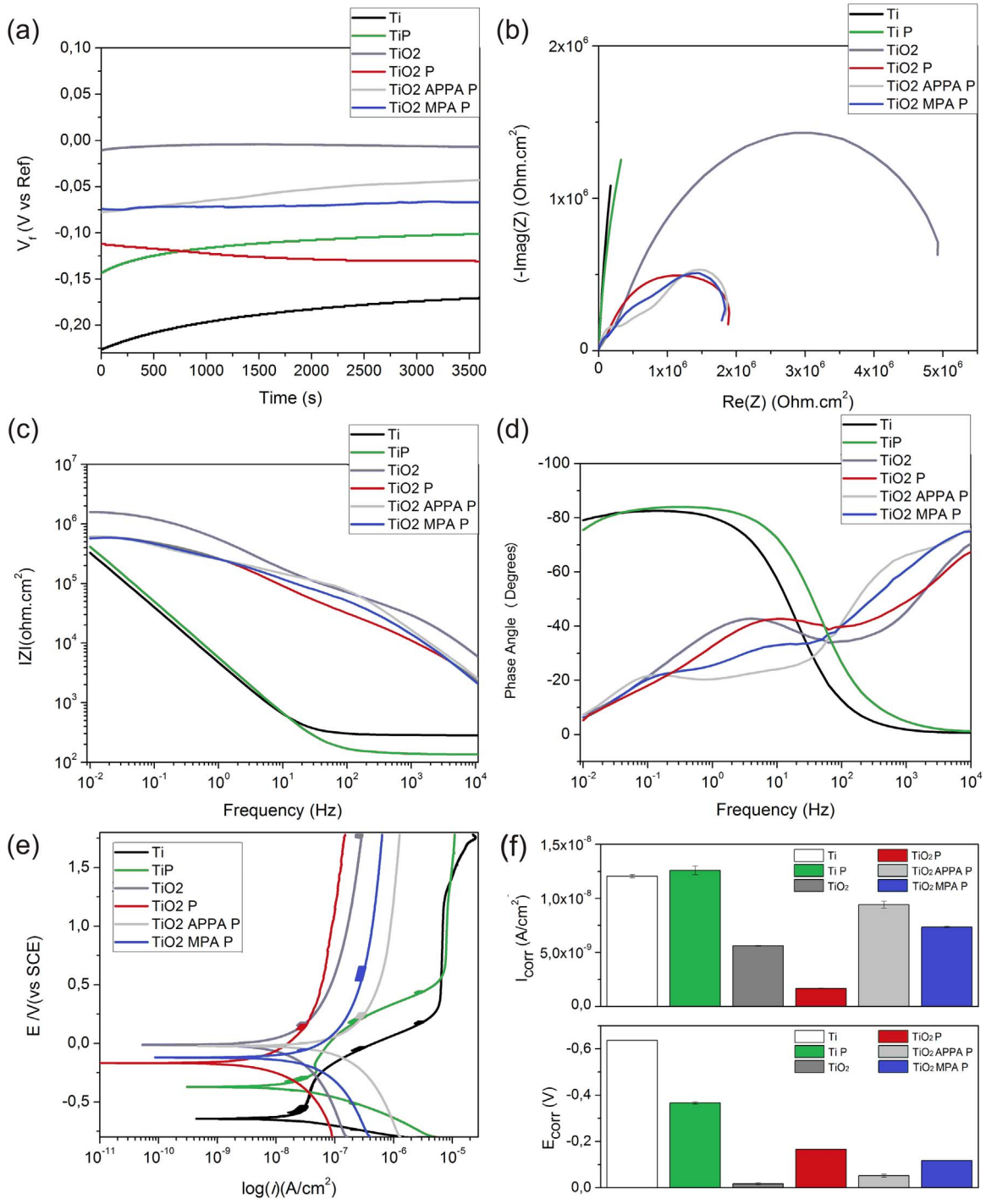

Fig. 5. Evolution OCP (a), EIS Nyquist plot (b), EIS Bode impedance plot (c), Bode Phase angle plot (d), polarization curves (e), E_{corr} and I_{corr} values (f) from corrosion analysis.

occurs in the surface under the exposed conditions. The higher potential presented for TiO_2 indicates that the sample has a higher corrosion resistance as compared to the other samples. This is due to the protective passive oxide layer on the surface. However, the samples functionalized with APPA, MPA, and the peptides also presented good corrosion resistance, − 0.04 V and − 0.06 V respectively. This noble resistance was better than that of the pristine titanium sample. The organic coatings provide a protection by preventing corrosive ions from approaching the surface. However, defects that lead to the degradation in the organic material due to water transport through the coating are common. Subsequently, damage from corrosion follows (Kelly et al., 2002; Wood, 2010).

Electrochemical Impedance Spectroscopy (EIS) results are shown in the Nyquist plot in Fig. 5**b**. Also displayed is the imaginary impedance (-Im(Z), (Ohm*cm^2)) versus the actual component of the impedance (Re (Z), (Ohm*cm^2)). In Fig. 5**b**, the Ti and Ti P samples presented large, incomplete semicircles, indicating a capacitive response. TiO_2, TiO_2 P, TiO_2 APPA P, and TiO_2 MPA P showed semi-arcs with a wider diameter for TiO_2. This indicates that the corrosion resistance for TiO_2 is higher due to the protective oxide layer present.

The Bode plot, represented by the Z modulus in the function of frequency (Fig. 5**c**), shows that the Ti sample reached 3.1 × 10^5 Ω cm^2 at a low frequency. However, the Z modulus of the functionalized surfaces was around 6.5 × 10^5 Ω cm^2, indicating that the functionalized

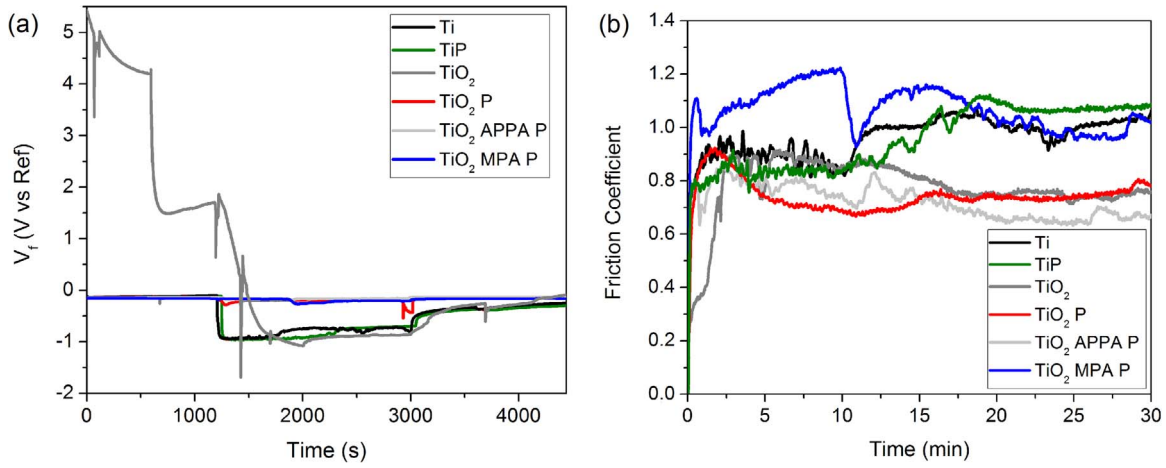

Fig. 6. Evolution of the free potential (OCP) (a) and coefficient of friction (b) measured during tribocorrosion experiments (sliding) for the samples analyzed.

samples with the spacers and DMP1 peptides have a better corrosion resistance.

The phase-angle plots can be classified into high and low-frequency regions. These regions provide the corrosion processes/kinetics at the surface layer(electrolyte) and the substrate(surface) layer interfaces, respectively (Srinivasan et al., 2015). An increase in phase-angle values (increased peak area) in the high-frequency region for TiO_2, TiO_2 P, TiO_2 APPA P, and TiO_2 MPA P can be attributed to the high corrosion resistance behavior (Fig. 5**d**).

The polarization curves obtained for the bio-functionalized surfaces are shown in Fig. 5**e**. Electrochemical behavior was analyzed by estimating corrosion current density (I_{corr}) and corrosion potential (E_{corr}). These were determined through Tafel extrapolation (Fig. 5**f**). Corrosion results indicated that the bio-functionalization had a significant influence on the E_{corr} and I_{corr} values, which resulted in the decrease of I_{corr} and the shift of E_{corr} values to noble potentials. The Ti E_{corr} increased from − 0.637 V to approximately − 0.015 V for TiO_2, − 0.050 V for TiO_2 APPA P, and − 0.120 V for TiO_2 MPA P. This is the result of a thick crystalline rutile TiO_2 film that provides more electrochemical stability versus the thin amorphous native oxide layer formed upon the pristine Ti. The I_{corr} is an important parameter for evaluating the corrosion reaction kinetics, as it directly indicates the corrosion rate, per Faraday's law. Hence, the lower current density implies a lower corrosion rate (Fu et al., 2015).

Overall, our data showed that surface bio-functionalization led to a decrease in current density. The samples TiO_2 APPA P and TiO_2 MPA P showed high I_{corr} values when compared to TiO_2. This is due to the presence of biomolecules, which can influence corrosion kinetics. However, it is still unclear whether biomolecules inhibit or accelerate electrochemical reactions. It is likely that different combinations of biomolecules and metals may present different ranges of effects (Royhman et al., 2014; Yan et al., 2006). The results represent a noble electrochemical potential for the bio-functionalized Ti samples, and they indicate an improved corrosion resistance and lower corrosion rate.

Equivalent circuit models were used to analyze EIS data, thereby estimating the total circuit resistance (R_t) and the total circuit capacitance (C_t) of the analyzed samples. In the circuit model, constant phase element (CPE) was used instead of ideal capacitors, due to the non-linear behavior in the Nyquist and Bode plots. The equivalent circuit models for each sample are shown at the Supporting information in Fig. S7.

Table S1 displays the total resistance and total capacitance, as well as χ^2 values determining the level of proper fit. The parameters indicated that the total resistance for the bio-functionalized samples is higher when compared to the pristine Ti. This denotes a more protective layer for the bio-functionalized samples. Further, there is a significant decrease in capacitance values for TiO_2, TiO_2 P, TiO_2 APPA P, and TiO_2 MPA P samples. This can be attributed to the presence of rutile titanium dioxide film and could indicate long-term stability for this film (Dolata et al., 1996).

3.3.2. Tribocorrosion

The tribocorrosion tests were performed at the free potential condition, and the evolution of electrochemical potential (OCP), as a function of time, is shown in Fig. 6**a**. For samples Ti and Ti P, a drop-in potential of approximately 0.8 V can be observed when the alumina ball (counter body) sliding starts on the surface. It indicates that the electrochemical nature of the Ti and Ti P samples under mechanical stimuli is inferior, and can possibly be linked to the higher level of degradation in their surfaces. The electrochemical potential stays at low values throughout the sliding phase, ranging from − 0.9 V to − 0.7 V, with some oscillations/cycling – usually attributed to depassivation/repassivation events.

The TiO_2 sample presented some magnetic field interferences, as shown in the spectra. Clearly, the electrochemical potential was higher for TiO_2 P. Moreover, functionalization with the oxide, organic and biomolecule, in TiO_2 APPA P and TiO_2 MPA P, significantly improved the performance of the metal under mechanical exposure. The initial potential is much higher for these samples, presenting a drop-in potential of only 0.05 V under mechanical sliding. This indicates some protection of the surface provided by the organic materials.

Inside the human body, tribochemical reactions in the metal on metal (MoM) joints result in the formation of a tribolayer on the CoCrMo alloy. This tribolayer consists of tribochemical products and a carbonaceous material originated from proteinaceous stemming from the synovial fluid (Mathew et al., 2014). The natural tribolayer is capable of improving the MoM implant performance by decreasing the total mass loss and reducing corrosion (Mathew et al., 2014). The samples containing the organic groups and the peptides (TiO_2 APPA P and TiO_2 MPA P) can mimic the formation of a tribolayer, thereby increasing corrosion resistance with less mass loss. Hence, the presence of DMP1 peptides enhances the stability of the material during tribocorrosion. The peptides that adhere to the surface can change their nature by transforming into a lubricous material, which protects the surface (Quiram et al., 2016; Mathew et al., 2012). Furthermore, the peptides may enhance the hardness and strength of the top surface, resulting in a decrease of the wear rate, besides the lubrication factor (Wang et al., 2016a, 2016b).

The coefficient of friction (COF) was another factor analyzed during the counter body sliding. Each of the curves (Fig. 6**b**) indicate that when the sliding starts, the coefficient of friction increases. This is due

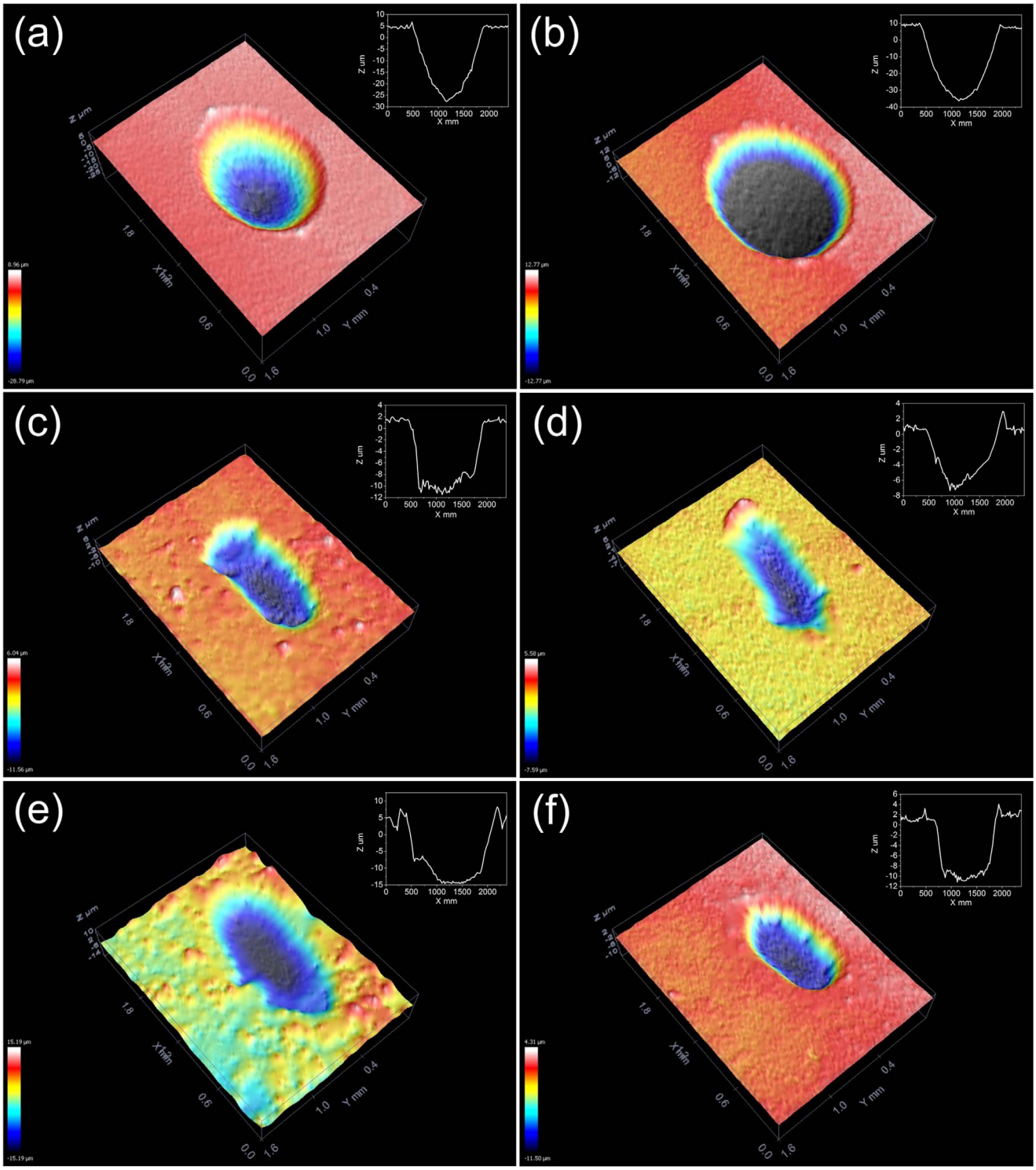

Fig. 7. Confocal 3D images showing the wear scar after tribocorrosion test for Ti (a), Ti P (b), TiO_2 (c), TiO_2 P (d), TiO_2 APPA P (e) and TiO_2 MPA P (f).

to the run-in period. However, after the initial period, the friction coefficient decreases and displays a nearly constant/stable value. The lubricating nature of organic molecules and peptides on the surface resulted in a significant decrease of the COF, except in the TiO_2 MPA P sample. The decrease in the COF around 12 min, for MPA P sample, may suggest that COF is dependent on the contact conditions and on the nature of the organic molecule that forms the lubricating complex. In this way, a drop in the COF could be affected by the shear-stress distribution and the microstructure of the surface (Wang et al., 2016a, 2016b).

The wear scar, present in the samples after tribocorrosion was analyzed by confocal optical microscopy (Fig. 7). It is possible to verify that Ti and Ti P groups showed an increased mass loss, with a wear track compatible with the sliding of the counter body (alumina ball). TiO_2-coated samples did not exhibit a deeper wear track (minor damage on the surface), thus indicating greater surface protection. The differences between the amorphous native oxide from Ti samples and the crystalline rutile oxide is a possible explanation for this dissimilar behavior. The rutile crystalline phase is associated with an increase in hardness up to 17 GPa (Alves et al., 2013).

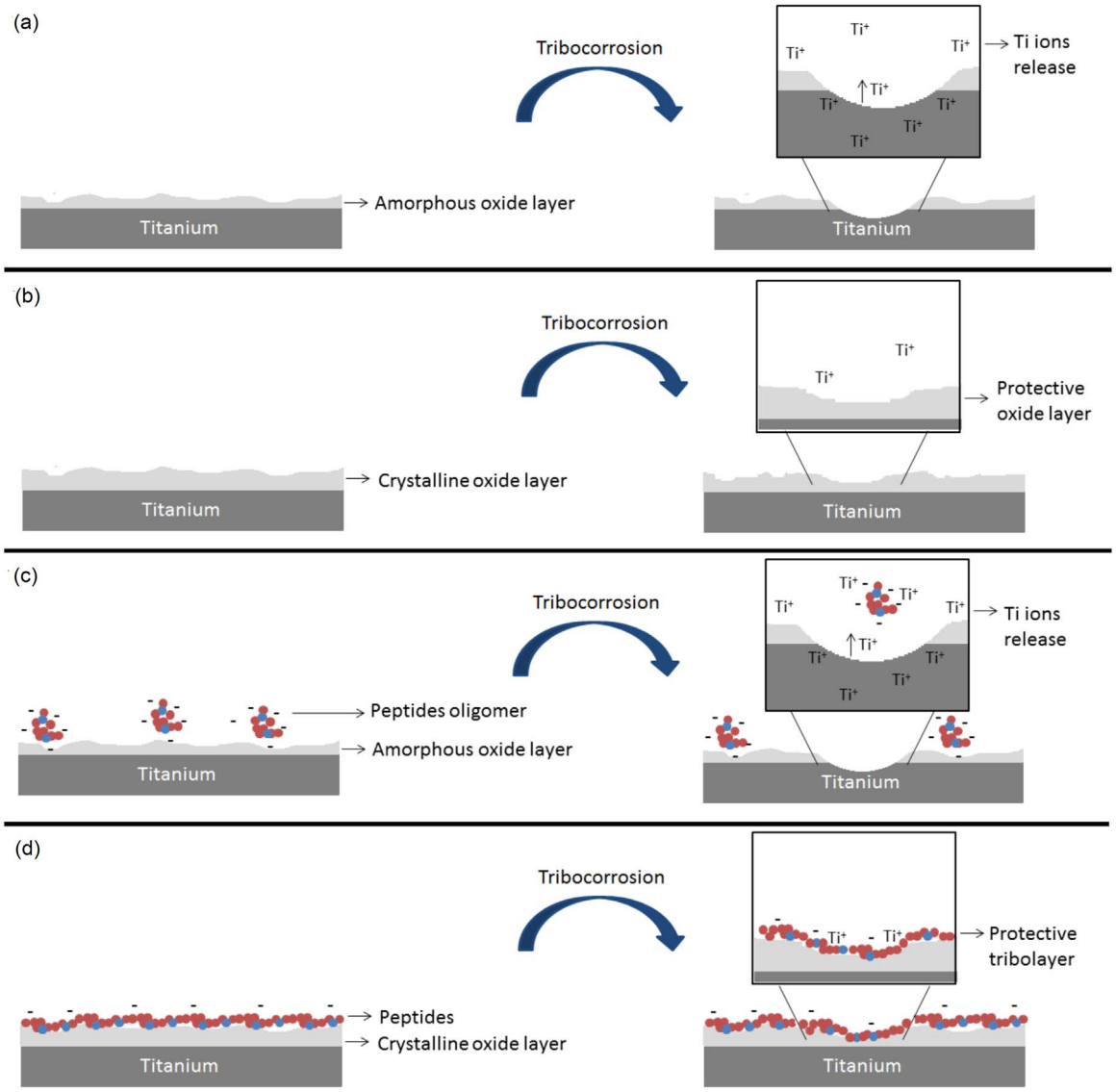

Fig. 8. Schematic diagram of possible tribocorrosion mechanisms that occur at the non-functionalized and the bio-functionalized tested surfaces: Ti (a), TiO_2 (b), Ti P (c), TiO_2 P, TiO_2 MPA P and TiO_2 APPA P (d).

The presence of the DMP1 peptides did not present significant differences as compared with the samples of TiO_2 P, TiO_2 APPA P, and TiO_2 MPA P, therefore they provided protection from the tribocorrosion exposure. However, in the Ti P sample, there was an increase in mass loss due to the sliding wear as compared to the Ti sample. This may result from the negative isoelectric point presented by the biomolecules at the pH of 7.4. At this pH the charge density for peptide pA is − 2 and for peptide pB is − 3 (Peptide Property Calculator, 2017). The negative isoelectric point attracts the positive metallic ions and transports them away from the implant surface (Williams, 2014). An interaction between the peptides and the metal ions consequently increases the rate of dissolution and circumvents the formation of the tribolayer (Sin et al., 2013). For samples modified with the oxide, the corrosion rate is lower for the passive layer and leads to the formation of complexes between the peptides and the ions. These complexes are deposited on the surface and act as a protective layer.

3.3.3. Possible tribocorrosion mechanism

The possible tribocorrosion mechanisms that occur at the non-functionalized and the bio- functionalized test surfaces are shown in Fig. 8. Pristine titanium samples possess a native amorphous oxide layer/film. However, during tribocorrosion, this oxide layer is worn out due to its thinness (less than 12–15 nm) and absence of crystallinity. Without the oxide layer, the metal surface is exposed. The result is a higher degree of mass loss (Fig. 8**a**).

Conversely, when the surface is coated with rutile TiO_2, the rutile layer slows down the degradation rate of the film. This contributes to the leveling-off of the wear track profiles (Oliveira et al., 2015), and results in a more protective oxide layer (Fig. 8**b**).

DMP1 peptides can act as a protective layer or they can increase the mass loss, depending on the physicochemical characteristics of the surface. For the titanium sample functionalized with DMP1 peptides (Ti P), the corrosion and mass loss averages are like those in the pristine titanium sample. This indicates an elevated level of corrosion and tribocorrosion behavior. This increased material degradation can be attributed to the peptides' isoelectric point at the tested electrolyte pH. DMP1 peptides form agglomerated regions upon the titanium surface, and once the PBS electrolyte pH reaches 7.4, the negatively charged peptides cluster with each other as oligomers. The negatively charged peptides attract titanium ions from the metal, thus increasing their diffusion rate, and consequently, the material degradation (Sin et al., 2013), (Fig. 8**c**).

Alternatively, when the DMP1 peptides adhered to samples functionalized with rutile TiO_2 and the spacer molecules (MPA or APPA), the corrosion rate and wear scars decrease. This indicates the formation of a protective tribofilm. DMP1 peptides adhere more effectively to TiO_2, TiO_2 MPA, and TiO_2 APPA surfaces through covalent bonds between the amino or acidic groups. These groups are present on the peptides and the –OH, -COOH, or $–NH_2$ terminal groups from the respective samples. This provides the formation of a stable layer, which may combine with the ions released during tribocorrosion. This stable layer maintains its stability and acts as a lubricous tribolayer that protects the surface (Fig. 8**d**).

3.4. Clinical implications

Although in vivo tests still need to be completed, the translation of these discoveries into clinical trials has promise. The bio-functionalized materials may provide an osteogenic surface which is capable of nucleating hydroxyapatite and remineralizing the bone tissue. Furthermore, the peptides derived from DMP1 can induce the formation of osteoblastic cells, which may lead to tissue regeneration. The bio-functionalization also has a positive influence on the material corrosion resistance and degradation. It reduces the release of metallic ions and debris, and thereby extends the implant lifetime by lowering the risk of infection.

4. Conclusions

This study provides a facile and efficient method of titanium functionalization with DMP1 peptides, further enhancing the biocompatibility, bioactivity, osteogenic capability, electrochemical, and mechanical aspects of these functional materials. Further, the beneficial effects of the treatment are increased with implant integration.

The bio-interfaces developed showed the capability of modulating cell affinity and proliferation, with enhanced results in the presence of the MPA spacer. Further, DMP1 peptides triggered osteoblastic differentiation, and, as a result, osteogenic surfaces were obtained. Additionally, DMP1 peptides, immobilized through MPA and APPA spacers, have the potential to stabilize calcium phosphate minerals with a Ca/P ratio near to that of hydroxyapatite. Electrochemical and mechanical results indicated an increase in the corrosion and tribo-corrosion resistance of the functionalized material. These findings suggest that the bio-functionalization of Ti substrates could advance regenerative medicine through advanced implants.

Acknowledgements

The authors would like to thank Maria João Runa for her advice regarding corrosion and tribocorrosion aspects and Dr. Cortino Sukotjo for his help during sample preparation. This work was financially supported by FAPESP (2013/07296-2; 2014/01713-3; 2014/27015-0; 2014/20471-0), NIH grant DE 11657 and the Brodie Endowment Fund.

Appendix A. Supporting information

Supplementary data associated with this article can be found in the online version at http://dx.doi.org/10.1016/j.jmbbm.2018.02.024.

References

Advincula, M., Fan, X., Lemons, J., Advincula, R., 2005. Surface modification of surface sol–gel derived titanium oxide films by self-assembled monolayers (SAMs) and non-specific protein adsorption studies. Colloids Surf. B Biointerfaces 42, 29–43. http://dx.doi.org/10.1016/j.colsurfb.2004.12.009.

Alla, A.P.R.K., Ginjupalli, K., Upadhya, N., Mohammed, S., Chandra sekar, R., Ravi, R. Krishna, 2011. Surface roughness of implants: a review. Trends Biomater. Artif. Organs 25, 112–118.

Alvares, K., 2014. The role of acidic phosphoproteins in biomineralization. Connect. Tissue Res. 55, 34–40. http://dx.doi.org/10.3109/03008207.2013.867336.

Alves, A.C., Oliveira, F., Wenger, F., Ponthiaux, P., Celis, J.-P., Rocha, L.A., 2013. Tribocorrosion behaviour of anodic treated titanium surfaces intended for dental implants. J. Phys. Appl. Phys. 46, 404001. http://dx.doi.org/10.1088/0022-3727/46/40/404001.

Alves, S.A., Bayón, R., de Viteri, V.S., Garcia, M.P., Igartua, A., Fernandes, M.H., Rocha, L.A., 2015. Tribocorrosion behavior of calcium- and phosphorous-enriched titanium oxide films and study of osteoblast interactions for dental implants. J. Bio- Tribo-Corros. 1, 1–21. http://dx.doi.org/10.1007/s40735-015-0023-y.

Alves, S.A., Patel, S.B., Sukotjo, C., Mathew, M.T., Filho, P.N., Celis, J.-P., Rocha, L.A., Shokuhfar, T., 2017. Synthesis of calcium-phosphorous doped TiO2 nanotubes by anodization and reverse polarization: a promising strategy for an efficient biofunctional implant surface. Appl. Surf. Sci. 399, 682–701. http://dx.doi.org/10.1016/j.apsusc.2016.12.105.

Askari, S., Ul Haq, A., Macias-Montero, M., Levchenko, I., Yu, F., Zhou, W., Ostrikov, K.K., Maguire, P., Svrcek, V., Mariotti, D., 2016. Ultra-small photoluminescent silicon-carbide nanocrystals by atmospheric-pressure plasmas. Nanoscale 8, 17141–17149. http://dx.doi.org/10.1039/c6nr03702j.

Balasundaram, G., Yao, C., Webster, T.J., 2008. TiO2 nanotubes functionalized with regions of bone morphogenetic protein-2 increases osteoblast adhesion. J. Biomed. Mater. Res. A 84, 447–453. http://dx.doi.org/10.1002/jbm.a.31388.

Bauer, S., Schmuki, P., von der Mark, K., Park, J., 2013. Engineering biocompatible implant surfaces: Part I: materials and surfaces. Prog. Mater. Sci. 58, 261–326. http://dx.doi.org/10.1016/j.pmatsci.2012.09.001.

Bedi, R.S., Zanello, L.P., Yan, Y., 2009. Osteoconductive and osteoinductive properties of zeolite MFI coatings on titanium alloys. Adv. Funct. Mater. 19, 3856–3861. http://dx.doi.org/10.1002/adfm.200901226.

Bhatia, A., Albazzaz, M., Espinoza Orías, A.A., Inoue, N., Miller, L.M., Acerbo, A., George, A., Sumner, D.R., 2012. Overexpression of DMP1 accelerates mineralization and alters cortical bone biomechanical properties in vivo. J. Mech. Behav. Biomed. Mater. 5, 1–8. http://dx.doi.org/10.1016/j.jmbbm.2011.08.026.

Cai, K., Frant, M., Bossert, J., Hildebrand, G., Liefeith, K., Jandt, K.D., 2006. Surface functionalized titanium thin films: zeta-potential, protein adsorption and cell proliferation. Colloids Surf. B Biointerfaces 50, 1–8. http://dx.doi.org/10.1016/j.colsurfb.2006.03.016.

Cölfen, H., 2010. Biomineralization: a crystal-clear view. Nat. Mater. 9, 960–961. http://dx.doi.org/10.1038/nmat2911.

Dolata, M., Kedzierzawski, P., Augustynski, J., 1996. Comparative impedance spectroscopy study of rutile and anatase Tio2 film electrodes. Electrochim. Acta 41, 1287–1293. http://dx.doi.org/10.1016/0013-4686(95)00449-1.

Dumont, V.C., Mansur, A.A.P., Carvalho, S.M., Medeiros Borsagli, F.G.L., Pereira, M.M., Mansur, H.S., 2016. Chitosan and carboxymethyl-chitosan capping ligands: Effects on the nucleation and growth of hydroxyapatite nanoparticles for producing biocomposite membranes. Mater. Sci. Eng. C 59, 265–277. http://dx.doi.org/10.1016/j.msec. 2015.10.018.

Enciso, M., Schütte, C., Site, L.D., 2015. Influence of pH and sequence in peptide aggregation via molecular simulation. J. Chem. Phys. 143, 243130. http://dx.doi.org/10.1063/1.4935707.

Frosch, K.-H., Sondergeld, I., Dresing, K., Rudy, T., Lohmann, C.H., Rabba, J., Schild, D., Breme, J., Stuermer, K.M., 2003. Autologous osteoblasts enhance osseointegration of porous titanium implants. J. Orthop. Res. Off. Publ. Orthop. Res. Soc. 21, 213–223. http://dx.doi.org/10.1016/S0736-0266(02)00143-2.

Fu, T., Zhan, Z., Zhang, L., Yang, Y., Liu, Z., Liu, J., Li, L., Yu, X., 2015. Effect of surface mechanical attrition treatment on corrosion resistance of commercial pure titanium. Surf. Coat. Technol. 280, 129–135. http://dx.doi.org/10.1016/j.surfcoat.2015.08.041.

Gajjeraman, S., Narayanan, K., Hao, J., Qin, C., George, A., 2007. Matrix Macromolecules in Hard Tissues Control the Nucleation and Hierarchical Assembly of Hydroxyapatite. J. Biol. Chem. 282, 1193–1204. http://dx.doi.org/10.1074/jbc.M604732200.

Gorski, J.P., 1992. Acidic phosphoproteins from bone matrix: a structural rationalization of their role in biomineralization. Calcif. Tissue Int. (50), 391–396. http://dx.doi.org/10.1007/BF00296767.

Gsponer, J., Vendruscolo, M., 2006. Theoretical approaches to protein aggregation. Protein Pept. Lett. 13, 287–293.

Hanawa, T., 2010. Biofunctionalization of titanium for dental implant. Jpn. Dent. Sci. Rev. 46, 93–101. http://dx.doi.org/10.1016/j.jdsr.2009.11.001.

He, G., Dahl, T., Veis, A., George, A., 2003. Nucleation of apatite crystals in vitro by self-assembled dentin matrix protein 1. Nat. Mater. 2, 552–558. http://dx.doi.org/10.1038/nmat945.

He, G., Gajjeraman, S., Schultz, D., Cookson, D., Qin, C., Butler, W.T., Hao, J., George, A., 2005. Spatially and temporally controlled biomineralization is facilitated by interaction between self-assembled dentin matrix protein 1 and calcium phosphate nuclei in solution. Biochemistry (Moscow) 44, 16140–16148. http://dx.doi.org/10.1021/bi051045l.

Ishizaki, T., Saito, N., Takai, O., 2010. Correlation of cell adhesive behaviors on superhydrophobic, superhydrophilic, and micropatterned superhydrophobic/superhydrophilic surfaces to their surface chemistry. Langmuir ACS J. Surf. Colloids 26, 8147–8154. http://dx.doi.org/10.1021/la904447c.

Jemat, A., Ghazali, M.J., Razali, M., Otsuka, Y., 2015. Surface modifications and their effects on titanium dental implants. BioMed. Res. Int. 2015, e791725. http://dx.doi.org/10.1155/2015/791725.

Kelly, R.G., Scully, J.R., Shoesmith, D., Buchheit, R.G., 2002. Electrochemical Techniques in Corrosion Science and Engineering. CRC Press.

Kowalczyńska, H.M., Nowak-Wyrzykowska, M., 2003. Modulation of adhesion, spreading and cytoskeleton organization of 3T3 fibroblasts by sulfonic groups present on polymer surfaces. Cell Biol. Int. 27, 101–114. http://dx.doi.org/10.1016/S1065-

6995(02)00290-1.
Kumari, A., Yadav, S.K., Yadav, S.C., 2010. Biodegradable polymeric nanoparticles based drug delivery systems. Colloids Surf. B Biointerfaces 75, 1–18. http://dx.doi.org/10.1016/j.colsurfb.2009.09.001.
Li, L.-H., Kong, Y.-M., Kim, H.-W., Kim, Y.-W., Kim, H.-E., Seong-Joo Heo, Koak, J.-Y., 2004. Improved biological performance of Ti implants due to surface modification by micro-arc oxidation. Biomaterials 25, 2867–2875.
López-Huerta, F., Cervantes, B., González, O., Hernández-Torres, J., García-González, L., Vega, R., Herrera-May, A.L., Soto, E., 2014. Biocompatibility and surface properties of TiO2 thin films deposited by DC magnetron sputtering. Materials 7, 4105–4117. http://dx.doi.org/10.3390/ma7064105.
Ma, Y., Dong, J., Bhattacharjee, S., Wijeratne, S., Bruening, M.L., Baker, G.L., 2013. Increased protein sorption in poly(acrylic acid)-containing films through incorporation of comb-like polymers and film adsorption at low pH and high ionic strength. Langmuir ACS J. Surf. Colloids 29, 2946–2954. http://dx.doi.org/10.1021/la305137m.
Mathew, M.T., Jacobs, J.J., Wimmer, M.A., 2012. Wear-corrosion synergism in a CoCrMo hip bearing alloy is influenced by proteins. Clin. Orthop. 470, 3109–3117. http://dx.doi.org/10.1007/s11999-012-2563-5.
Mathew, M.T., Nagelli, C., Pourzal, R., Fischer, A., Laurent, M.P., Jacobs, J.J., Wimmer, M.A., 2014. Tribolayer formation in a metal-on-metal (MoM) hip joint: an electrochemical investigation. J. Mech. Behav. Biomed. Mater. 29, 199–212. http://dx.doi.org/10.1016/j.jmbbm.2013.08.018.
McKenna, J., Patel, J., Mitra, S., Soin, N., Švrček, V., Maguire, P., Mariotti, D., 2011. Synthesis and surface engineering of nanomaterials by atmospheric-pressure microplasmas. Eur. Phys. J. Appl. Phys. 56, 24020. http://dx.doi.org/10.1051/epjap/2011110203.
Molina, J., Esteves, M.F., Fernández, J., Bonastre, J., Cases, F., 2011. Polyaniline coated conducting fabrics. Chemical and electrochemical characterization. Eur. Polym. J. 47, 2003–2015. http://dx.doi.org/10.1016/j.eurpolymj.2011.07.021.
Moulder, J.F., 1992. Handbook of X-ray Photoelectron Spectroscopy: a Reference Book of Standard Spectra for Identification and Interpretation of XPS Data, Physical Electronics Division. Perkin-Elmer Corporation.
Oliveira, F.G., Ribeiro, A.R., Perez, G., Archanjo, B.S., Gouvea, C.P., Araújo, J.R., Campos, A.P.C., Kuznetsov, A., Almeida, C.M., Maru, M.M., Achete, C.A., Ponthiaux, P., Celis, J.-P., Rocha, L.A., 2015. Understanding growth mechanisms and tribocorrosion behaviour of porous TiO2 anodic films containing calcium, phosphorous and magnesium. Appl. Surf. Sci. 341, 1–12. http://dx.doi.org/10.1016/j.apsusc.2015.02.163.
Oskam, G., Nellore, A., Penn, R.L., Searson, P.C., 2003. The growth kinetics of TiO2 nanoparticles from titanium(IV) alkoxide at high water/titanium ratio. J. Phys. Chem. B. 107, 1734–1738. http://dx.doi.org/10.1021/jp021237f.
Padovano, J.D., Ravindran, S., Snee, P.T., Ramachandran, A., Bedran-Russo, A.K., George, A., 2015. DMP1-derived peptides promote remineralization of human dentin. J. Dent. Res. 94, 608–614. http://dx.doi.org/10.1177/0022034515572441.
Peptide Property Calculator, (n.d.). 〈https://www.genscript.com/tools/peptide-property-calculator〉 (Accessed 15 December 2017).
Quiram, G., Gindri, I.M., Kerwell, S., Shull, K., Mathew, M.T., Rodrigues, D.C., 2016. Nanoscale mechanical evaluation of electrochemically generated tribolayer on CoCrMo alloy for hip joint application. J. Bio- Tribo-Corros. 2, 15. http://dx.doi.org/10.1007/s40735-016-0045-0.
Rabe, M., Verdes, D., Seeger, S., 2011. Understanding protein adsorption phenomena at solid surfaces. Adv. Colloid Interface Sci. 162, 87–106. http://dx.doi.org/10.1016/j.cis.2010.12.007.
Rafieerad, A.R., Ashra, M.R., Mahmoodian, R., Bushroa, A.R., 2015. Surface characterization and corrosion behavior of calcium phosphate-base composite layer on titanium and its alloys via plasma electrolytic oxidation: a review paper. Mater. Sci. Eng. C 57, 397–413. http://dx.doi.org/10.1016/j.msec. 2015.07.058.
Ramel, C.F., Lüssi, A., Özcan, M., Jung, R.E., Hämmerle, C.H.F., Thoma, D.S., 2016. Surface roughness of dental implants and treatment time using six different implantoplasty procedures. Clin. Oral. Implants Res. 27, 776–781. http://dx.doi.org/10.1111/clr.12682.
Ravindran, S., George, A., 2014. Multifunctional ECM proteins in bone and teeth. Exp. Cell Res. 325, 148–154. http://dx.doi.org/10.1016/j.yexcr.2014.01.018.
Royhman, D., Radhakrishnan, R., Yuan, J.C.-C., Mathew, M.T., Mercuri, L.G., Sukotjo, C., 2014. An electrochemical investigation of TMJ implant metal alloys in an artificial joint fluid environment: the influence of pH variation. J. Cranio-Maxillo-Fac. Surg. Off. Publ. Eur. Assoc. Cranio-Maxillo-Fac. Surg. 42, 1052–1061. http://dx.doi.org/10.1016/j.jcms.2014.01.029.
Ruan, J., Wang, X., Yu, Z., Wang, Z., Xie, Q., Zhang, D., Huang, Y., Zhou, H., Bi, X., Xiao, C., Gu, P., Fan, X., 2016. Enhanced physiochemical and mechanical performance of chitosan-grafted graphene oxide for superior osteoinductivity. Adv. Funct. Mater. 26, 1085–1097. http://dx.doi.org/10.1002/adfm.201504141.
Sangeetha, S., Kathyayini, S.R., Raj, P.D., Dhivya, P., Sridharan, M., 2013. Biocompatibility studies on TiO2 coated Ti surface, in: Proceedings of International Conference on Advance Nanomaterials and Emerging Engineering Technologies, ICANMEET, 2013, pp. 404–408. 〈http://dx.doi.org/10.1109/ICANMEET.2013.6609330〉.
Sezin, M., Croharé, L., Ibañez, J.C., 2016. Microscopic study of surface microtopographic characteristics of dental implants. Open Dent. J. 10, 139–147. http://dx.doi.org/10.2174/1874210601610010139.
Shi, L., Wang, F., Zhu, W., Xu, Z., Fuchs, S., Hilborn, J., Zhu, L., Ma, Q., Wang, Y., Weng, X., Ossipov, D.A., 2017. Self-healing silk fibroin-based hydrogel for bone regeneration: dynamic metal-ligand self-assembly approach. Adv. Funct. Mater. http://dx.doi.org/10.1002/adfm.201700591.
Silva-Bermudez, P., Rodil, S.E., 2013. An overview of protein adsorption on metal oxide coatings for biomedical implants. Surf. Coat. Technol. 233, 147–158. http://dx.doi.org/10.1016/j.surfcoat.2013.04.028.
Silva-Bermudez, P., Muhl, S., Rodil, S.E., 2013. A comparative study of fibrinogen adsorption onto metal oxide thin films. Appl. Surf. Sci. 282, 351–362. http://dx.doi.org/10.1016/j.apsusc.2013.05.133.
Sin, J.R., Hu, X., Emami, N., 2013. Tribology, corrosion and tribocorrosion of metal on metal implants. Tribol. - Mater. Surf. Interfaces 7, 1–12. http://dx.doi.org/10.1179/1751584X13Y.0000000022.
Srinivasan, A., Shin, K.S., Rajendran, N., 2015. Applications of dynamic electrochemical impedance spectroscopy (DEIS) to evaluate protective coatings formed on AZ31 magnesium alloy. RSC Adv. 5, 29589–29593. http://dx.doi.org/10.1039/C4RA16967K.
Suh, K.Y., Seong, J., Khademhosseini, A., Laibinis, P.E., Langer, R., 2004. A simple soft lithographic route to fabrication of poly(ethylene glycol) microstructures for protein and cell patterning. Biomaterials 25, 557–563.
Sun, Y.-S., Chang, J.-H., Huang, H.-H., 2016. Enhancing the biological response of titanium surface through the immobilization of bone morphogenetic protein-2 using the natural cross-linker genipin. Surf. Coat. Technol. 303 (Part A), 289–297. http://dx.doi.org/10.1016/j.surfcoat.2016.02.051.
Tanaka, Y., Doi, H., Kobayashi, E., Yoneyama, T., Hanawa, T., 2007. Determination of the immobilization manner of amine-terminated poly(ethylene glycol) electrodeposited on a titanium surface with XPS and GD-OES. Mater. Trans. JIM 48, 287–292. http://dx.doi.org/10.2320/matertrans.48.287.
Tanaka, Y., Saito, H., Tsutsumi, Y., Doi, H., Imai, H., Hanawa, T., 2008. Active hydroxyl groups on surface oxide film of titanium, 316L stainless steel, and cobalt-chromium-molybdenum alloy and its effect on the immobilization of poly(ethylene glycol). Mater. Trans. 49, 805–811. http://dx.doi.org/10.2320/matertrans.MRA2007317.
Tobin, E.J., 2017. Recent coating developments for combination devices in orthopedic and dental applications: a literature review. Adv. Drug Deliv. Rev. http://dx.doi.org/10.1016/j.addr.2017.01.007.
Trino, L.D., Dias, L.F.G., Albano, L.G.S., Bronze-Uhle, E.S., Rangel, E.C., Graeff, C.F.O., Lisboa-Filho, P.N., 2018. Zinc oxide surface functionalization and related effects on corrosion resistance of titanium implants. Ceram. Int. http://dx.doi.org/10.1016/j.ceramint.2017.11.195.
Wang, C., Bai, Y., Bai, Y., Gao, J., Ma, W., 2016. Enhancement of corrosion resistance and bioactivity of titanium by Au nanoparticle-loaded TiO2 nanotube layer. Surf. Coat. Technol. 286, 327–334. http://dx.doi.org/10.1016/j.surfcoat.2015.12.051.
Wang, Z., Yan, Y., Su, Y., Qiao, L., 2016. Effect of proteins on the surface microstructure evolution of a CoCrMo alloy in bio-tribocorrosion processes. Colloids Surf. B Biointerfaces 145, 176–184. http://dx.doi.org/10.1016/j.colsurfb.2016.05.002.
Williams, D., 2014. Essential Biomaterials Science. Cambridge University Press.
Wood, R.J.K., 2010. 2.15 - Tribocorrosion. In: Richardson, Tony J.A. (Ed.), Shreirs Corrosion, 1st ed. Oxford Elsevier, pp. 1005–1050.
Yan, Y., Neville, A., Dowson, D., Williams, S., 2006. Tribocorrosion in implants—assessing high carbon and low carbon Co–Cr–Mo alloys by in situ electrochemical measurements. Tribol. Int. 39, 1509–1517. http://dx.doi.org/10.1016/j.triboint.2006.01.016.
Zhang, B., Kong, T., Xu, W., Su, R., Gao, Y., Cheng, G., 2010. Surface functionalization of zinc oxide by carboxyalkylphosphonic acid self-assembled monolayers. Langmuir 26, 4514–4522. http://dx.doi.org/10.1021/la9042827.
Zheng, C., Wang, J., Liu, Y., Yu, Q., Liu, Y., Deng, N., Liu, J., 2014. Functional selenium nanoparticles enhanced stem cell osteoblastic differentiation through BMP signaling pathways. Adv. Funct. Mater. 24, 6872–6883. http://dx.doi.org/10.1002/adfm.201401263.